

# Electrochemical Synthesis and Photocatalytic Property of Zinc Oxide Nanoparticles

Kodihalli G. Chandrappa, Thimmappa V. Venkatesha\*

(Received 5 December 2011; accepted 7 February 2012; published online 29 February 2012.)

**Abstract:** Zinc oxide (ZnO) nanoparticles of varying sizes (20, 44 and 73 nm) have been successfully synthesized by a hybrid electrochemical-thermal method using aqueous sodium bicarbonate electrolyte and sacrificial Zn anode and cathode in an undivided cell under galvanostatic mode at room temperature. The as-synthesized product was characterized by X-ray diffraction (XRD), X-ray photoelectron spectra (XPS), Scanning electron microscopy along with Energy dispersive analysis of X-ray (SEM/EDAX), Transmission electron microscopy (TEM), Ultra Violet - Diffuse reflectance spectroscopic methods (UV-DRS). and UV-DRS spectral methods. The as-synthesized compound were single-crystalline and Rietveld refinement of calcined samples exhibited hexagonal (Wurtzite) structure with space group of  $P6_3mc$  (No.186). The band gaps for synthesized ZnO nanoparticles were 3.07, 3.12 and 3.13 eV, respectively, based on the results of diffuse reflectance spectra (DRS). The electrochemically synthesized ZnO powder was used as photocatalysts for UV-induced degradation of Methylene blue (MB). Photodegradation was also found to be function of exposure time and dye solution pH. It has been found that as-synthesized powder has excellent photocatalytic activity with 92% degradation of MB, indicating ZnO nanoparticles can play an important role as a semiconductor photocatalyst.

**Keywords:** Zinc Oxide; Methylene Blue; Photocatalytic activity; Semiconductor

**Citation:** Kodihalli G. Chandrappa and Thimmappa V. Venkatesha, "Electrochemical Synthesis and Photocatalytic Property of Zinc Oxide Nanoparticles", *Nano-Micro Lett.* 4 (1), 14-24 (2012). <http://dx.doi.org/10.3786/nml.v4i1.p14-24>

## Introduction

Nanostructured semiconductor oxides are of great importance for several technological applications because of their several interesting optical and electronic properties. The design and fabrication of nanostructured semiconductor metal oxides with a tunable physico-chemical property for advanced catalytic applications have drawn a great deal of attention in the field of catalysis [1-4]. Several semiconductor oxides such as zinc oxide (ZnO),  $TiO_2$ ,  $SnO_2$  and  $ZrO_2$  have been found to be attractive photocatalysts because they are environmentally sustainable with high catalytic efficiency in the degradation of various environmental pollutants such as pesticides, detergents, dyes and volatile organic compounds into carbon dioxide and water un-

der UV light irradiation [5-8]. Among these semiconductor oxides, use of ZnO as a photocatalyst is preferred because it has a comparable band gap (3.2 eV) with relatively large quantum efficiency [9] in comparison to other commonly used photo-catalysts. Also, it has great potential applications in room-temperature UV lasers [10], sensors [11] and photocatalysis [4, 12] due to its unique electrical and optical properties such as low dielectric constant, high chemical stability, good photoelectric and piezoelectric behaviors [13]. In addition, it has been largely emphasized in the literature that the physico-chemical properties of these semiconductor oxides such as ZnO can be suitably tailored according to our application since there exists a relationship between their size and the catalytic efficiency [14-17]. Gouvea et al. [18] used three methods to prepare nano-ZnO,

Department of P. G. Studies & Research in Chemistry, School of Chemical Sciences, Jnana Sahyadri campus, Kuvempu University, Shankaraghatta-577451, Shimoga, Karnataka, India.

\*Corresponding author. E-mail: drtvvenkatesha@yahoo.co.uk

and the results indicating that the smaller particle size could lead to higher photocatalytic activity.

ZnO has received significant importance in the field of photocatalysis because of its large exciton binding energy (60 meV) at room temperature [10], high optical activity, photochemical stability, high surface energy and also cheap and non-toxic in nature [19]. Also, the potential of electron derived from ZnO is more negative than that generated by most-investigated TiO<sub>2</sub> for photocatalytic reduction reaction [4]. When ZnO is irradiated under a light with energy equal to or higher than its band gap, it generates electron-hole pair which then participates in the photocatalytic process. In addition, the higher photocatalytic activity of ZnO is also attributed to the large number of defects such as oxygen vacancies, interstitial zinc atom from the donor states, while zinc vacancies and interstitial oxygen atoms from the acceptor states [20].

It has been found that the physico-chemical properties of ZnO and hence its application significantly depends on its synthesis route. In literature, there are large number of reports for the synthesis of nanostructured ZnO such as precipitation/mechanical milling [21], microemulsion [22], ultrasonic radiation [23], microwave irradiation [24], solution combustion, microwave assisted solvothermal [25] and sol-gel method [26]. However, in recent years, the electrochemical method of synthesis of nanosized metal oxide powder and films have acquired a considerable interest because of its simplicity, low operating temperature and viability in commercial production. Recently, ZnO and CuO nanocrystals have been successfully synthesized by electrochemical route [27, 28]. Thus, designing a suitable method for preparing ZnO at ambient temperature with narrow particle size distribution, better properties and less operating cost is a challenge for researchers.

The increase in human population has resulted in the development of large-scale industries such as textile and paper industries whose waste products represent a major environmental hazard to aquatic biota and humans due to their toxicity [29] and the tendency to cause eutrophication [5]. Detection and removal of these toxic chemicals is a major challenge in convention methods. Thus, there is an urgent need of eco-friendly technologies for the detection and removal of textile effluents from water. It has been shown that dyes can be easily adsorbed and catalyzed on oxide surfaces. However, to the best of our knowledge, there exist only a few reports [30-33] which intend to directly remove commonly used industrial dyes. The present investigation is focused on the bulk synthesis and characterization of ZnO nanoparticles by electrochemical route without using any template or surfactant at room temperature. Also, we have discussed in detail spectroscopic detection (and quantification) of commonly used textile dye (Methylene Blue; cationic) in aqueous solution using

these ZnO nanoparticles as a function of various parameters.

## Experimental Procedure

### Starting Materials and Synthesis of ZnO Nanoparticles

Zinc metal plate (99.99%), sodium bicarbonate (AR grade: 99.5%) purchased from Sisco Research laboratories, Mumbai and Methylene Blue (MB) from S. D. Fine Chemicals Ltd., India, were used as received. Millipore water (specific resistance, 15 M $\Omega$  cm at 25°C, Millipore Elix 3 water purification system, France) was used to prepare the electrolyte solution. In a typical synthesis, ZnO nanoparticles are synthesized using a standard electrochemical technique mentioned in ref [27]. Prior to electrolysis, the Zn plates were activated by immersing in dilute HCl (1 M) for 30 sec followed by washing with Millipore water. The electrolyte consisted of 400 ml, 30 mM (1.008 gm) NaHCO<sub>3</sub> solution which was taken in a rectangular undivided cell having dimension 5×6×0.8 cm<sup>3</sup> with Zn plates as both cathode and anode. The electrolysis was carried out for about one hour under galvanostatic conditions where the constant current was drawn from a DC power supply (model PS 618 potentiostat/galvanostat 302/2 A supplied by Chem link, Mumbai) with constant stirring at 800 rpm. The pH of the electrolyte was recorded before and after electrolysis. The particles were filtered and isolated from the solution. The same procedure was also repeated using 60 and 120 mM of NaHCO<sub>3</sub>. The resulting particles were calcined at different temperature ranging from 60°C to 600°C for 1 h.

### Catalyst characterization

General morphology, structure, crystallite size, oxidation state, compositional analysis and band gaps of the nanoparticles were performed using powder X-ray diffraction (XRD), transmission and scanning electron microscopy, energy dispersive X-ray analyzer (EDAX), X-ray photoelectron spectra (XPS) and UV-DRS spectroscopy. Morphology and compositional analysis were carried out in a scanning electron microscope (SEM, Philips XL 30) fitted with an EDAX in the voltage range of 200–300 kV. Transmission electron microscope (TEM) images of selected samples were recorded (Model: JEOL 2000 FX-II) with an acceleration voltage of 200 kV. 2  $\mu$ l of ZnO – ethanol solution was dropped on a Cu grid with a carbon-reinforced plastic film. XRD patterns (X'pert Pro Diffractometer, Phillips, Cu K $\alpha$  radiation, ( $\lambda_{Cu}$ =1.5418 Å) working at 30 mA and 40 kV) were recorded in the 2 $\theta$  range from 10° to 90° at a scanning rate of 1° min<sup>-1</sup>. For Rietveld refinement analysis, XRD data was refined using

the FullProf Suite-2000 version. The average crystallite sizes were estimated using Scherrer equation [34]. The X-ray photoelectron spectra (XPS) were recorded by Thermo-Scientific Multilab 2000 equipment employing Al  $K_{\alpha}$  X-rays at 150 W. The absorption, reflectance and DRS spectra on ZnO nanoparticles were studied using UV-DRS absorption spectroscopy (Specord S600-212C205 UV Spectrophotometer) and dye adsorption kinetics on ZnO nanoparticles were studied using Spectrum, SP-2102 UVPC, UV-Vis Spectrophotometer (path length=1 cm). Dye adsorption kinetics were carried out using ZnO nanoparticles (100 mg) of varying sizes which were added to 100 ml (50 ppm, say) of dye solution and stirred continuously for 2 h for homogeneity. Aliquots were collected from the reaction beaker at regular time intervals and concentration of dye in solution and degradation ratio was plotted as a function of time by monitoring the changes in the  $\lambda_{\max}$  line intensity with time.

### Photocatalytic Degradation of Dye in Aqueous Solution

In order to evaluate the photocatalytic activity of the samples, photodegradation of MB dye under UV light irradiation was carried out in presence of ZnO nanoparticles at room temperature. Photocatalysis experiments were carried out with ZnO (100 mg in 100 ml of dye solution) and MB dye (10 ppm, 30ppm and 50 ppm) solution of three different concentrations prepared by dissolving appropriate amount of MB dye in Millipore water. The photochemical reactor used in this study was made of a Pyrex glass jacketed quartz tube. A high pressure mercury vapor lamp (HPML) of 125 W (Philips, India) was placed inside the jacketed quartz tube. To avoid fluctuations in the input light intensity, a supply ballast and capacitor were connected in series with the lamp. Water was circulated through the annulus of the quartz tube to avoid heating of the solution. Reaction suspension was prepared by adding 100 mg of ZnO sample into a 250 ml beaker containing 100 ml of MB (10-50 ppm) dye solution. Prior to illumination, the suspension was magnetically stirred for 2 h in dark to establish an absorption/desorption equilibrium of MB and also to ensure that the suspension of the catalyst was uniform. Subsequently, the dispersion containing MB and photocatalyst (ZnO) was irradiated under UV light. The lamp radiated predominantly at 365 nm corresponding to energy of 3.4 eV and photon flux of  $5.8 \times 10^{-6}$  mol of photons  $\text{sec}^{-1}$ . The MB-ZnO solution mixture was repeatedly illuminated for 10 min at 2 min intervals. During the 2 min interval, 3 ml of aliquots were taken from the test mixture. Due to progressive degradation of the dye with consecutive flashes, the color of the solution mixture (as well as aliquots) changed from blue to light blue followed by white. The change in color of the dye solution as a function of time

was monitored by using UV-Vis spectroscopy.

## Results and Discussion

### XRD to Study ZnO Nanostructure

The powder XRD patterns of as-prepared and calcined compounds of ZnO nanoparticles are shown in Fig. 1. It can be seen from Fig. 1(a) that, the seven peaks appeared at  $2\theta$  of  $13.1^\circ$ ,  $24.1^\circ$ ,  $27.9^\circ$ ,  $30.9^\circ$ ,  $32.9^\circ$ ,  $53.9^\circ$  and  $59.6^\circ$ , corresponding to the characteristic peaks of zinc hydroxy carbonate, and is in accordance with standard JCPDS file no. 72-1100. Similar observation was also made by Siqingaowa et al. [35]. Also, the other small peaks appearing at  $2\theta$  of  $34.4^\circ$ ,  $36.2^\circ$  and  $47.4^\circ$  values corresponds to characteristic peaks of ZnO. The XRD patterns for the calcined samples at  $300^\circ\text{C}$  for 1 h (Fig. 1(b)), could be completely indexed to hexagonal phase (JCPDS file No. 36-1451). The crystallite size ( $d$ ) estimated from the full width at half maximum ( $w$ ) of the dominant (101) peak at diffraction angle  $2\theta \approx 36.2^\circ$  using Scherrer's equation was found to be 44 nm. In Fig. 1(a), the diffracted lines were broad, less intense and corresponded to the zinc hydroxy carbonate and ZnO. On increasing calcination temperature from 300 to  $600^\circ\text{C}$ , the characteristic ZnO peaks become sharper and the crystallinity increased [35]. The powder XRD pattern for the sample calcined at  $600^\circ\text{C}$  is given in Fig. 1(c). From the XRD data, the average crystallite sizes were found to be 20, 44 and 73 nm respectively (Table 1). It clearly indicates that, an increase in calcination temperature brings about a corresponding increase on crystallite sizes of ZnO nanoparticles, leading to sharper diffraction peaks.

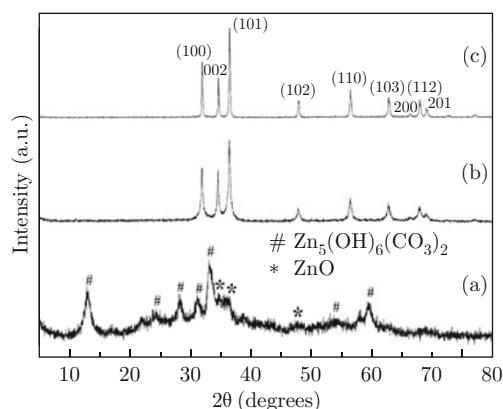


Fig. 1 XRD patterns of (a) ZnO precursor obtained from the bath concentration at 30 mM  $\text{NaHCO}_3$  at  $1 \text{ A/dm}^2$ , and calcined for 1 h at different temperature (b)  $300^\circ\text{C}$  and (c)  $600^\circ\text{C}$ .

The preferred orientation of ZnO nanoparticles was estimated from the XRD data according to the methodology developed by Berube and L Esperance [36], where the texture coefficient ( $T_c$ ) is calculated by using the

**Table 1** Electrolysis parameter and process efficiency for the preparation of ZnO nanoparticles.

Temperature (°C)	Crystallite size (nm)									Average
	Family of crystallographic planes $\{hkl\}$									
	{100}	{002}	{101}	{102}	{110}	{103}	{200}	{112}	{201}	
As-prepared	21	18	10	0	0	0	0	0	31	20
300	49	71	63	65	34	40	24	24	21	44
600	49	99	62	103	88	57	77	58	68	73

equation below:

$$T_c = \frac{I_{(hkl)}}{\sum I_{(hkl)}} \times \frac{\sum I_{0(hkl)}}{I_{0(hkl)}} \quad (1)$$

where,  $I_{(hkl)}$  is the diffraction line intensity of the  $(hkl)$  reflection of ZnO powder,  $\sum I_{(hkl)}$  is the sum of the intensities of all the diffraction lines monitored. The  $I_0$  refers to intensity of the reference ZnO sample (JCPDS file No. 36-1451). Figure 2 shows the texture coefficient of ZnO sample obtained from electrolyte concentration of 30 mM and current density of 1.0 A/dm<sup>2</sup>. It can be seen that the majority of the ZnO crystallites are oriented parallel to the (002) plane.

The structural parameters for all the calcined samples were refined using Rietveld refinement method.

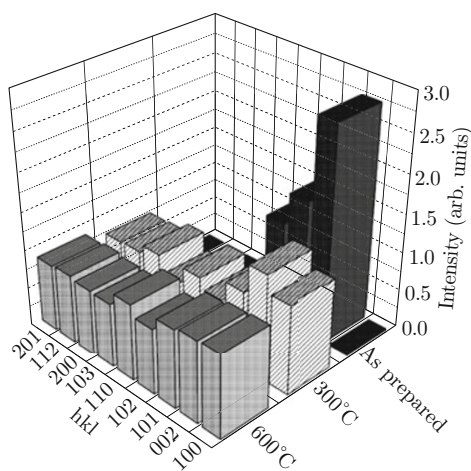


Fig. 2 Texture Coefficient of ZnO nanoparticles obtained from 30 mM NaHCO<sub>3</sub> at 1 A/dm<sup>2</sup>, calcined for 1 h at different temperature.

**Table 2** Rietveld refined structural parameters for ZnO nanoparticles synthesized by electrochemical method.

Atoms	Oxidation state	Wyckoff notations	x	y	z	B <sub>iso</sub>	Occupancy
Zn	2	(2b)	0.333 30	0.666 70	0.000 0	0.025	1
O	-2	(2b)	0.333 30	0.666 70	0.382 00	0.500	1

Crystal system=Hexagonal, Lattice parameters;  $a=3.252(2)$ ,  $c=5.208(6)$ ; Space group=P6<sub>3</sub> mc (No. 186);  $R$  factors (%),  $R_p=6.86$ ,  $R_{wp}=9.37$ ,  $R_{Bragg}=2.98$ ,  $R_F=1.78$ .

All the ZnO nanoparticles crystallized in the hexagonal (Wurtzite) structure with space group of P6<sub>3</sub>mc (No. 186). The refined structural parameters for ZnO calcined at 600°C for 1 h is given in Table 2. The observed lattice parameters agreed well with the reported standard JCPDS file No. 36-1451. Observed, calculated XRD patterns and their difference are given in Fig. 3, and there is good agreement between them. Further, we did not see any appreciable change in the lattice parameters on samples calcined to low temperature.

### Surface Composition and Oxidation States

The surface composition and oxidation states of the materials are deciding factors which play very important role in the process of catalytic reaction since they

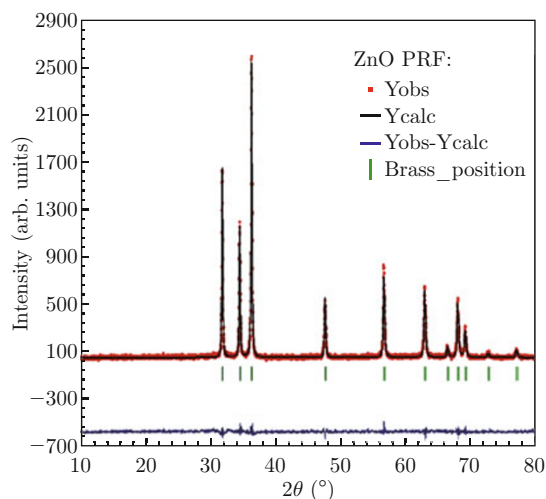


Fig. 3 Observed, calculated and the difference XRD patterns for the ZnO sample obtained from 30 mM NaHCO<sub>3</sub>, 1 A/dm<sup>2</sup>, calcined at 600°C for 1 h.

can strongly affect the catalytic activity. The photocatalytic activities of metal oxides are closely related with their surface structures. The surface composition and oxidation states of ZnO (hexagonal) were investigated by X-ray photoelectron spectroscopy (XPS). Figure 4 shows the XPS spectra of ZnO nanoparticles obtained from 30 mM NaHCO<sub>3</sub> at 1 A/dm<sup>2</sup> and calcined at 600°C for 1 h. It can be seen that the whole region of XPS spectra contains characteristic peaks of Zn (2*p*) and O (1*s*) (Fig. 4(a) and 4(b)). The Zn (2*p*) signal could be deconvoluted into two peaks (Fig. 4(a)). The binding energies obtained in the XPS analysis are corrected for specimen charging by calibrating the C(1*s*) peak at 285.4 eV and are accurate within ±0.1 eV. The binding energy at about 1022.18 eV is attributed to Zn 2*p*<sub>3/2</sub> and the 1045.37 eV is attributed to Zn 2*p*<sub>1/2</sub>, respectively, which are very close to the data for Zn (2*p*) in ZnO. Also, the Zn 2*p*<sub>3/2</sub> peaks are very sharp, this confirms that Zn atom is in the form of Zn<sup>2+</sup> state in ZnO sample. As shown in Fig. 4(b), the O (1*s*)

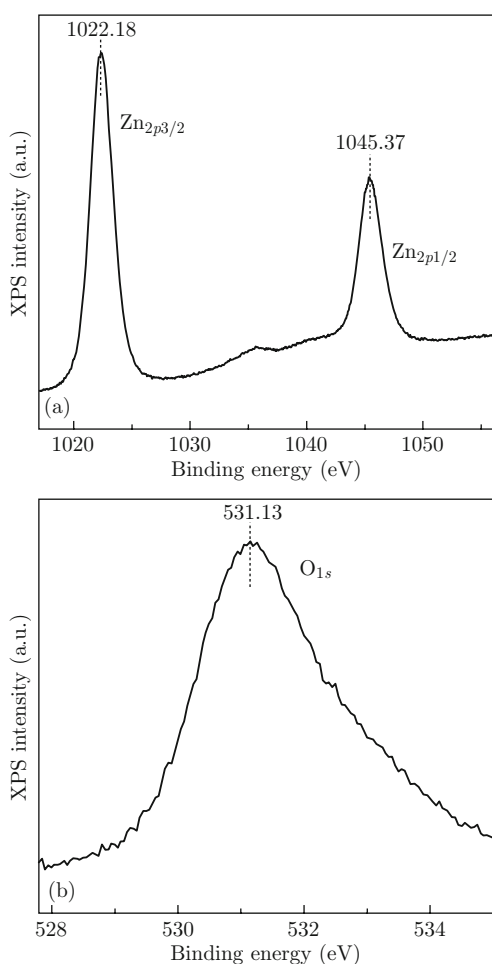


Fig. 4 X-ray photoelectron spectrum of (a) Zn2*p* and (b) O1*s* for ZnO nanoparticles obtained from 30 mM NaHCO<sub>3</sub> at 1 A/dm<sup>2</sup> and calcined at 600°C for 1 h.

core-level spectrum is broad, and these peaks ranging from 527 to 535 eV. The peak profile for O (1*s*) region is centered at about 531.13 eV and is due to oxygen present in the crystalline ZnO nanoparticles and can be indexed to the O<sup>2-</sup> in the ZnO. The inner electrons of Zn atoms are more clustered by the atomic nucleus, due to high density of oxygen atoms, which is beneficial to the increase of binding energy on XPS spectrum. The peak area of Zn (2*p*) and O (1*s*) cores were measured and it was used to calculate the chemical composition of the sample. Thus, the XPS spectra demonstrate that the synthesized materials are composed of ZnO nanoparticles.

### SEM/EDAX and TEM Analysis

Scanning electron micrographs and EDAX spectrum of as-prepared and calcined compounds of ZnO nanoparticles are shown in Fig. 5. Figure 5(a) shows the SEM image of as-prepared ZnO powder. It can be seen that the particles are agglomerated producing flower like structure, whereas the ZnO samples calcined at 300°C showed less randomly distributed small spindle shaped particles (Fig. 5(b)). The samples calcined at 600°C showed well defined and randomly oriented spindle like ZnO with somewhat compact structure (Fig. 5(c)). The flower like structure of as-prepared ZnO converted to spindle like structure on heating to 300°C. As the temperature is increased, the particles tend to grow as expected. The EDAX spectrum is shown in Fig. 5(d) indicates the presence of only Zinc and Oxygen, suggesting that the nanoparticles are indeed made up of Zn and O, the inset shows the ratio of zinc and oxygen ion concentration. The spectrum was devoid of any other metal ions indicating the purity of the samples.

The TEM images of ZnO nanoparticles obtained from the electrolyte concentration of (a) 30 mM and (b) 60 mM NaHCO<sub>3</sub> at 1 A/dm<sup>2</sup> and calcined at 600°C for 1 h are given in Fig. 6. It can be observed that ZnO nanoparticles are present as granules with spindle like shapes and are crystalline in nature. In Fig. 6(a) and 6(b) emphasize the particles have a clear spindle like morphology, and it was found that the average particles size ranging from 30-40 nm and these values are in good agreement with the values obtained from XRD data by Debye-Scherrer equation.

### UV-DRS Spectroscopy

Figure 7(a) shows the UV-Vis absorption, (b) reflectance and (c) diffuse reflectance spectra (DRS) of as-prepared and calcined ZnO nanoparticles to study their photoabsorption ability which is obtained from the 30 mM NaHCO<sub>3</sub> at 1 A/dm<sup>2</sup>. In Fig. 7(a), the absorption peaks are ascribed in between 330 to 380 nm,

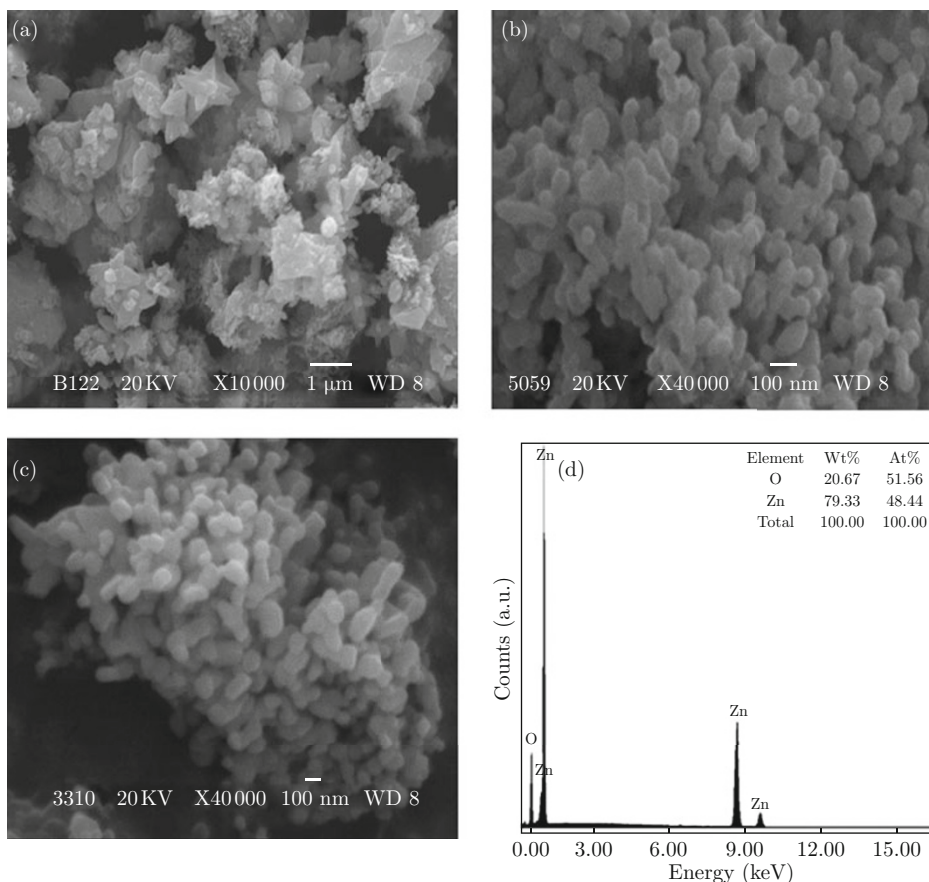


Fig. 5 SEM and EDAX analysis of ZnO nanoparticles obtained from 30 mM NaHCO<sub>3</sub> at 1 A/dm<sup>2</sup> calcined at different temperature for 1 h, (a) as-prepared ZnO, (b) 300 °C, (c) 600 °C and (d) EDAX pattern of ZnO calcined at 600 °C.

on increasing calcination temperature, the ZnO particles growth will takes place and the corresponding absorption band ( $\lambda_{\max}$ ) increases. The band gap ( $E_g$ ) of ZnO nanoparticles were calculated by using  $E_g = hc/\lambda$ , where  $h$ =plank's constant,  $c$ =velocity of light and  $\lambda$ =wavelength. The band gap values were lies in the range 3.34 to 3.42 eV (Table 3). The reflectance peaks (Fig. 7(b)) corresponding to ZnO sample showed the wavelength from 325 to 400 nm. The corresponding band gap was found to be 3.28 to 3.41 eV (Table 3). The optical absorbance properties of the ZnO samples were measured by diffuse reflectance spectroscopy (DRS) at room temperature. As displayed in Fig. 7(c), the absorption edges of ZnO nanoparticles were at about 363, 374 and 380 nm, respectively. Surprisingly, the absorption edge of ZnO nanoparticles shows an obvious blue shift. To obtain the optical band gap ( $E_g$ ) of ZnO nanoparticles, the absorbance coefficient ( $\alpha$ ) was calculated from the corresponding spectrum. The  $E_g$  values were thus determined by extrapolation of the linear portion of the  $(\alpha h\nu)^2$  curve versus the photon energy  $h\nu$  to  $(\alpha h\nu)^2=0$ . The corresponding band gap energies were determined and was found to be 3.07, 3.12, 3.13 eV for ZnO nanoparticles (Table 3). Thus, the present electrochemical-thermal method produces ZnO

nanoparticles which are in the blue region compared to the bulk ZnO (3.2 eV).

**Table 3**  $E_g$  values for the different ZnO nanoparticles obtained from UV-Vis absorption, reflectance spectroscopy and DRS.

Synthesized ZnO material	Abs. peak position (eV)	Rfn. peak position (eV)	$E_g$ (eV), from DRS
As-prepared compound	3.42	3.41	3.13
Calcined at 300 °C	3.41	3.31	3.07
Calcined at 600 °C	3.34	3.28	3.12

## Evaluation of Photocatalytic Activity

### Photocatalytic performance of ZnO with MB

The successful synthesis of ZnO nanoparticles offers an opportunity to examine their photocatalytic activity. The as-prepared and calcined ZnO nanoparticles were selected for the evaluation of photocatalytic activity with MB dye under the illumination of UV light. In order to study the effect of the UV light on the degradation of MB dye, a blank experiment was performed

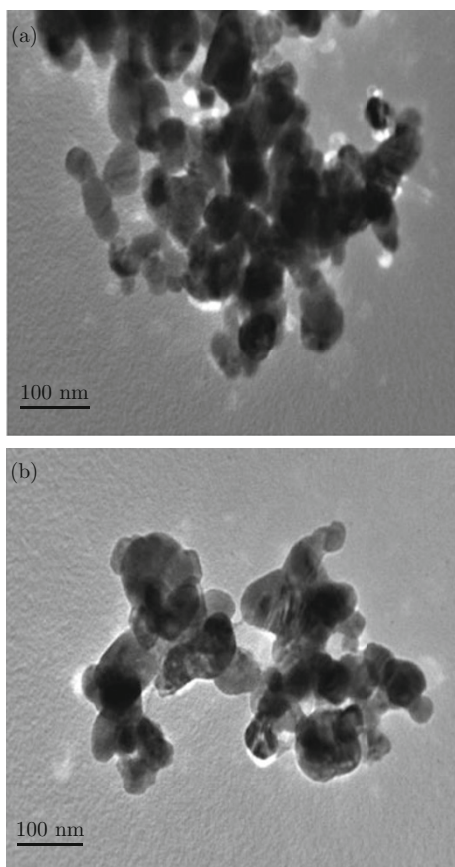


Fig. 6 TEM images of ZnO nanoparticles obtained from (a) 30 mM  $\text{NaHCO}_3$  and (b) 60 mM  $\text{NaHCO}_3$  at 1  $\text{A}/\text{dm}^2$  calcined at 600 °C for 1 h.

under UV light without the addition of photocatalysts (ZnO), which verified that MB dye of 10 mg/L was photolyzed up to 5% in 2 h. This degradation efficiency was negligible when the different sized particles were added to the solution. When there was no UV light, the concentration of MB dye with the addition of ZnO photocatalysts remains unchanged for 2 h. From these blank experiments, it can be concluded that UV light and photocatalysts are the necessary factors in the photocatalytic process. MB dye absorbs the light in the visible region (550-700 nm) with the absorption maxima at 664 nm. A series of experiments were carried out with different sized ZnO nanoparticles in MB dye solution. The time-dependent UV-Vis spectra of MB dye solution containing as-prepared ZnO nanoparticles, before and after irradiation interval of 100 min with UV light, are illustrated in Fig. 8. It can be seen that the intensity of absorption peak corresponding to the MB molecules at 664 nm decreases with increase in the exposure time and decreased to <50% at an irradiation time of 40 min. After irradiation under UV light for an hour ( $t=100$  min), the absorption peak shifted towards 635 nm, showing hypsochromic shift of 29 nm. The hypsochromic shift indicated that the photodegradation of MB dye under UV light irradiation proceeded

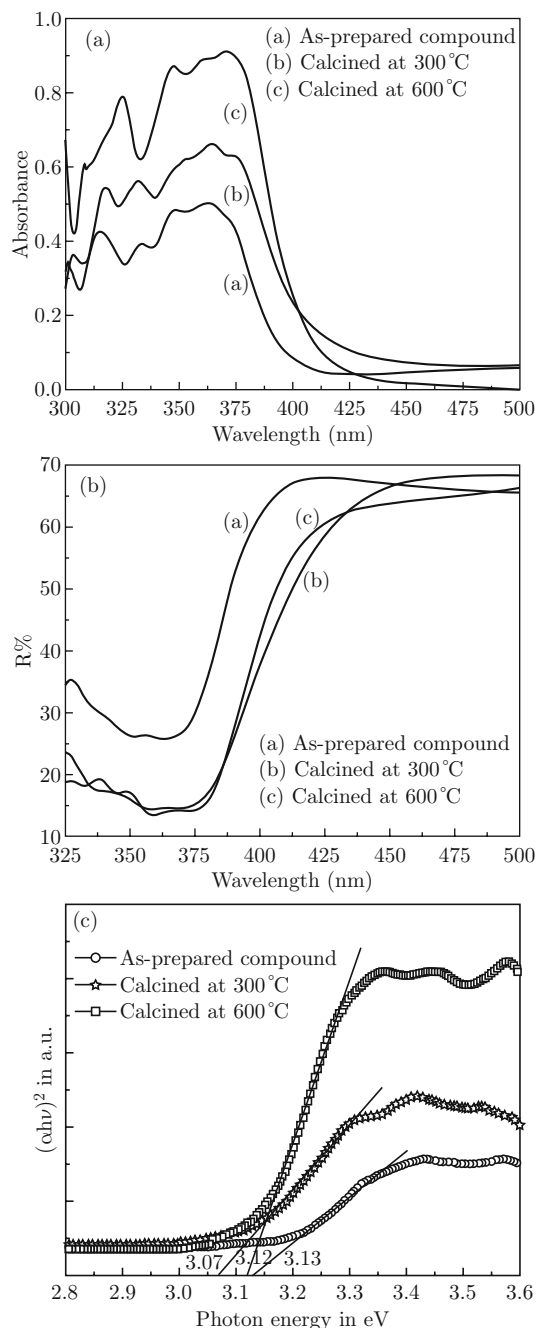


Fig. 7 UV-Vis absorption and DRS spectra of as-prepared and calcined ZnO nanoparticles obtained from 30 mM  $\text{NaHCO}_3$  at 1  $\text{A}/\text{dm}^2$ : (a) absorption, (b) reflectance and (c) DRS spectra.

through a continuous removal of methyl groups with extending the irradiation time.

#### Effect of Initial dye concentration with ZnO photocatalyst

Figure 9 shows the effect of initial dye concentration on the rate of exposure time by varying the dye concentration from 10 to 50 ppm with different sizes of ZnO photocatalyst (20-73 nm). The results revealed that

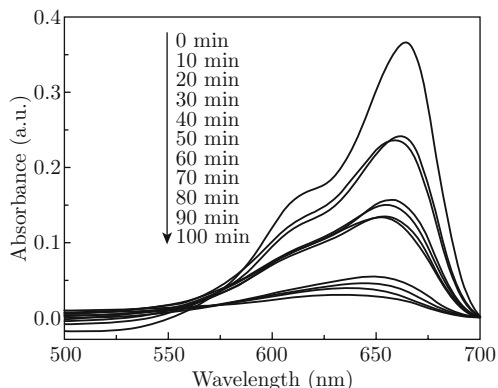


Fig. 8 Time-dependent absorption spectra of the MB solution during UV light irradiation in presence of as-prepared ZnO nanoparticles.

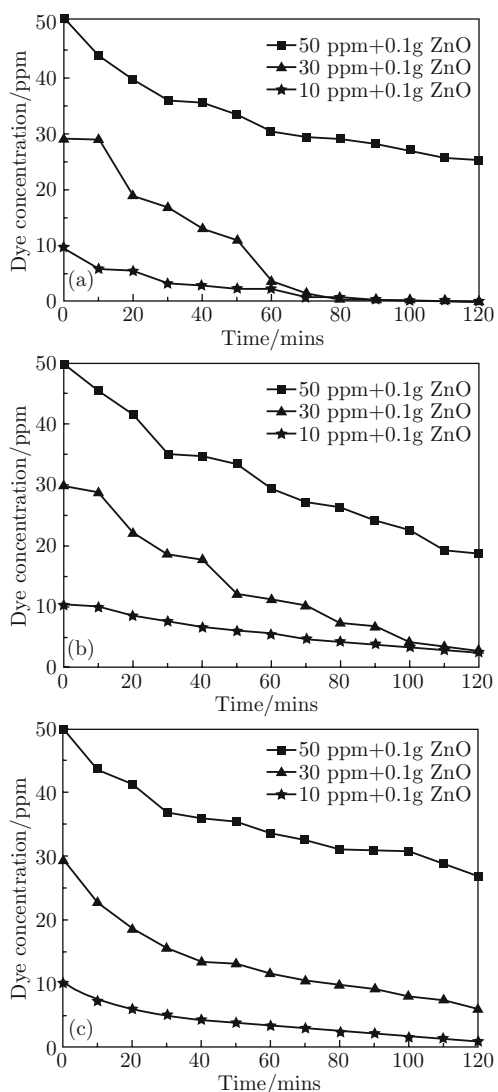


Fig. 9 Photocatalysis of MB dye concentration (10-50ppm in 100 ml of solution) with time as a result of different ZnO (1 g/L) photocatalysts (a) as-prepared, (b) calcined at 300°C and (c) calcined at 600°C (time span: 120 min).

the initial dye concentration influences the degradation efficiency severely. It can be seen that, the photodegra-

ation processes completed within 100 min in all the three different sizes of ZnO photocatalysts (Fig. 9). The percentage of photodegradation increases with increase in irradiation time. This suggests that the as-prepared and calcined (600°C) ZnO nanoparticles are exceedingly efficient substrates for degradation of azo-dyes such as MB.

### Influence of calcination temperature on the photocatalytic property of ZnO nanoparticles

The particle size and BET surface area affected the efficiency of nano ZnO due to variation in the calcination temperature (Table 4). The particle size will increase with increase in calcination and a drop in surface area; accompanied by a drop in photocatalytic activity; this suggests that, in addition to surface area, the morphology of nano ZnO (the particle size and crystallinity) also plays a crucial role in deciding the catalyst performance. The degradation efficiencies of different ZnO photocatalysts and different MB dye concentrations are shown in Fig. 10. It can be observed from Fig. 10(a), there is a special trend in the as-prepared ZnO nanoparticles. In the initial 70 min, the degradation efficiency reached the highest value of 85%. Afterward, the curve ascends tardily up to 92%. The crucial degradation efficiency after 100 min illumination has changed a little compared to the efficiency obtained after the initial 30 min illumination. The degradation efficiency of ZnO nanoparticles calcined at different temperature reduced in the order, 60>300>300°C. The relative bigger size and the reduction of the number of surface hydroxyl are the main reasons for the decrease of degradation efficiency of photocatalysts.

Table 4 Comparison of different ZnO photocatalysts.

Photocatalyst (Synthesized material)	Calcination temperature (°C)	Average particle size (nm)	BET surface area ( $\text{m}^2 \text{g}^{-1}$ )
As-prepared ZnO	60	20±2	19
Calcined ZnO	300	44±2	14
Calcined ZnO	600	73±2	11

However, a higher catalytic activity is observed in case of as-prepared ZnO sample only in the early stage of reaction (70 min), while the activity is decreased for longer time degradation. This evidence can be ascribed to the photocorrosion phenomenon in ZnO nanoparticles [37]. The increase of calcination temperature at 600°C (Fig. 10(c)), the increase of particle size and has increase in crystallinity which is helpful to enhance the photocatalytic activity. From this approach, the photocatalysts calcined at 600°C would be a relatively better sample for anti-photocorrosion. This suggests that

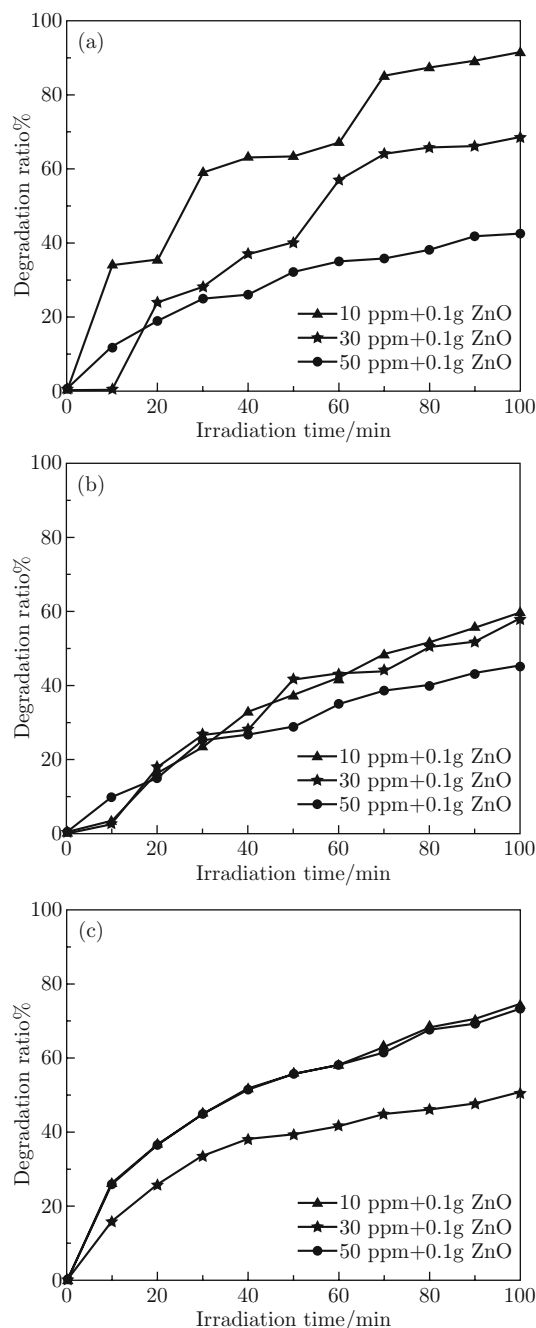


Fig. 10 Degradation ratio vs. Irradiation time for different ZnO photocatalysts [(a) as-prepared, (b) calcined at 300°C, (c) calcined at 600°C: 1 g/L] and different concentration of MB dye.

as-prepared and calcined (600°C) ZnO nanoparticles are highly efficient photocatalyst for degradation of MB dye.

#### Effect of pH on degradation of MB with ZnO photocatalyst

The effect of pH values on the degradation efficiency was studied in the pH values of 5 and 9 at the initial dye concentration of 50 ppm. Figure 11(a) and 11 (b)

shows the photocatalytic degradation of MB dye as a function of pH and exposure times. The Effect of pH on the photodegradation of MB dye was investigated over the pH range of 5-9, and the reaction pH was altered to study the photodegradation taking place on the surface of photocatalyst, since pH can alter the surface charge properties of the photocatalyst. From Fig. 11(a), in acidic solutions (pH=5.0) the degradation rate becomes slower and degree of degradation was lower in case of as-prepared compound but in calcined samples the degradation rate somewhat higher in the same irradiation time. A steady increase in the degradation of MB dye is observed at pH 9.0 (Fig. 11(b)). Higher the pH value can provide higher concentration of hydroxyl ions to react with holes ( $h^+$ ) to form hydroxyl radicals ( $OH\cdot$ ), subsequently enhancing the photodegradation rate of MB dye. It indicates that, the smaller particle size, higher crystallinity of photocatalyst and alkaline pH of reaction mixture has good photocatalytic activity for MB dye degradation under UV light irradiation.

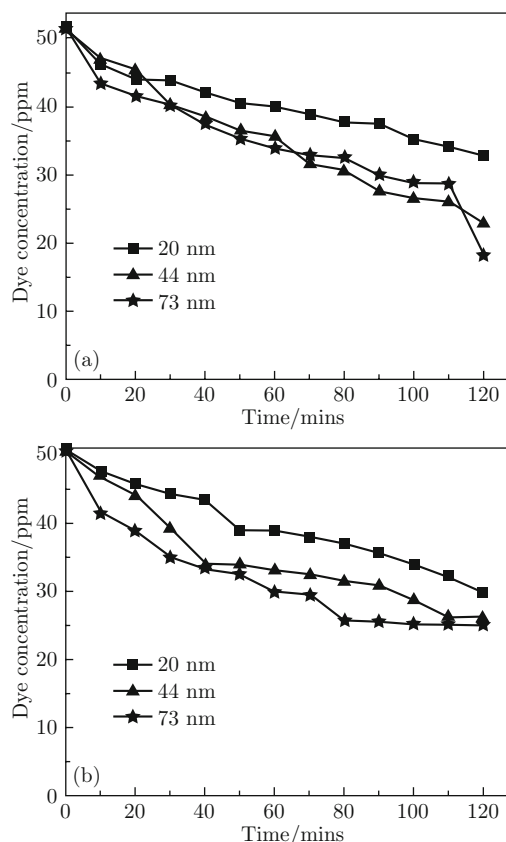


Fig. 11 Dye concentration vs. Irradiation time for different ZnO photocatalysts (20 nm, 44 nm and 73 nm: 1 g/L) and at different pH (a) 5 and (b) 9 (initial concentration of MB: 50 mg/l).

#### Conclusions

In the present work, the nanosized ZnO particles were

successfully generated by hybrid electrochemical-thermal method using  $\text{NaHCO}_3$  electrolyte without zinc salts, templates or surfactants. The  $\text{Zn}^{2+}$  ions generated at the sacrificial Zn electrode were converted into ZnO during electrolysis. The size range of the generated ZnO powder was 20-73 nm. The nanoparticles morphology was similar for all the samples obtained at different current densities and the size and shape does not depend on current density. The EDAX spectrum showed 100% ZnO compound in the calcined particles. TEM images confirmed the spindle like shape of ZnO nanoparticles and are well crystallized in the nanosize of 30-40 on nanometer scale. The band gap was higher for synthesized ZnO particles than their bulk counterparts. The yield of ZnO at  $1 \text{ A/dm}^2$  is maximum for 1 h electrolysis in all concentration of  $\text{NaHCO}_3$ . The method could be effectively used to synthesize ZnO on large scale. Also, we have presented here through systematic studies and performance of different sizes of ZnO nanoparticles in quantification and photocatalytic degradation of MB dye in aqueous solution. The higher photocatalytic property was probably caused by the smaller particle size, higher crystallinity and alkaline pH. These results show that the as-prepared and calcined ( $600^\circ\text{C}$ ) ZnO photocatalyst and the alkaline pH have a higher photocatalytic activity against UV light irradiation.

## Acknowledgments

The authors thank Kuvempu University, Shimoga, Prof. A. J. Bhattacharyya and S. S. Mandal SSCU, IISc, Bangalore, for providing the lab facilities to bring about this work. KGC and TVV thank, respectively the CSIR, New-Delhi for SRF [Sanction No. 09/908(0002) 2K9-EMR-I] and DST [No. S.R/S3/ME/014/2007], Government of India (GOI) for research grant.

## References

- [1] Y. H. Zheng, L. Zheng, Y. Y. Zhan, X. Y. Lin, Q. Zheng and K. Wei, *Inorg. Chem.* 46, 6980 (2007). <http://dx.doi.org/10.1021/ic700688f>
- [2] G. Colon, M. C. Hidalgo, J. A. Navio, E. P. Melian, O. G. Diaz and J. M. Dona, *Appl. Catal. B Environ* 78, 176 (2008). <http://dx.doi.org/10.1016/j.apcatb.2007.09.019>
- [3] H. G. Kim, P. H. Borse, W. Choi and J.S. Lee, *Angew. Chem. Int. Ed* 44, 4585 (2005). <http://dx.doi.org/10.1002/anie.200500064>
- [4] G. Marci, V. Augugliaro, M. J. Lopez-Munoz, C. Martin, L. Palmisano, V. Rives, M. Schiavello, R.J.D. Tilley and A. M. Venezia, *J. Phys. Chem. B* 105, 1026, 1033 (2001).
- [5] M. R. Hoffmann, S. T. Martin, W. Y. Choi and D. W. Bahnemann, *Chem. Rev.* 95, 69 (1995). <http://dx.doi.org/10.1021/cr00033a004>
- [6] T. Sehili, P. Boule and J. Lemaire, *J. Photochem, Photobiol. A. Chem.* 50, 103 (1989).
- [7] J. Villasenor, P. Reyes and G. Pecchi, *J. Chem. Technol. Biotechnol.* 72, 105 (1998). [http://dx.doi.org/10.1002/\(SICI\)1097-4660\(199806\)72:2<<\\$105::AID-JCTB883>>\\$3.0.CO;2-0](http://dx.doi.org/10.1002/(SICI)1097-4660(199806)72:2<<$105::AID-JCTB883>>$3.0.CO;2-0)
- [8] M. D. Driessen, T. M. Miller and V. H. Grassian, *J. Mol. Catal. A. Chem.* 131, 149 (1998). [http://dx.doi.org/10.1016/S1381-1169\(97\)00262-8](http://dx.doi.org/10.1016/S1381-1169(97)00262-8)
- [9] M. A. Behnajady, N. Modirshahla and R. Hamzavi, *J. Hazard. Mater. B* 133, 226 (2006). <http://dx.doi.org/10.1016/j.jhazmat.2005.10.022>
- [10] M. H. Huang, S. Mao, H. Feick, H. Q. Yan, Y. Y. Wu, H. Kind, E. Weber, R. Russo and P. D. Yang, *Science* 292, 1897 (2001). <http://dx.doi.org/10.1126/science.1060367>
- [11] E. Comini, G. Faglia, G. Sberveglieri, Z. W. Pan and Z. L. Wang, *Appl. Phys. Lett.* 81, 1869 (2003). <http://dx.doi.org/10.1063/1.1504867>
- [12] D. Han, X. L. Ren, D. Chen, F. Q. Tang, D. Wang and J. Ren, *Photogr. Sci. Photochem.* 23, 414 (2005).
- [13] X. Y. Kong and Z. L. Wang, *Nano. Lett.* 3, 1625 (2003). <http://dx.doi.org/10.1021/nl034463p>
- [14] S. J. Li, Z. C. Ma, J. Zhang and J. Z. Liu, *Catal. Commun.* 9, 1482 (2008). <http://dx.doi.org/10.1016/j.catcom.2007.12.016>
- [15] Q. Zhang, W. Fan and L. Gao, *Appl. Catal. B- Environ.* 76, 168 (2007). <http://dx.doi.org/10.1016/j.apcatb.2007.05.024>
- [16] L. Q. Jing, B. F. Xin, F. L. Yuan, L. P. Xue, B. Q. Wang and H. G. Fu, *J. Phys. Chem. B* 110, 17860 (2006). <http://dx.doi.org/10.1021/jp063148z>
- [17] N. Pradhan, A. Pal and T. Pal, *Langmuir* 17, 1800 (2001). <http://dx.doi.org/10.1021/la000862d>
- [18] C. A. K. Gouvea, F. Wypych and S. G. Moraes, *Chemosphere* 40, 433 (2000). [http://dx.doi.org/10.1016/S0045-6535\(99\)00313-6](http://dx.doi.org/10.1016/S0045-6535(99)00313-6)
- [19] K. R. Lee, S. Park, K. W. Lee and J. H. Lee, *J. Mater. Sci. Lett.* 22, 65 (2003). <http://dx.doi.org/10.1023/A:1021738526590>
- [20] R. Ullah and J. Dutta, *2nd Inter. Conf. Emerging Tech.* 353 (2006).
- [21] H. M. Deng, J. Ding, Y. Shi, X. Y. Liu and J. Wang, *J. Mater. Sci.* 36, 3273 (2001). <http://dx.doi.org/10.1023/A:1017902923289>
- [22] X. Jiaqiang, P. Qingyi, S. Yuan and L. Zhanchai, *Chin. J. Inorg. Chem.* 14, 355 (1998). (in Chinese)
- [23] W. Wenliang, L. Dongsheng, H. Xiangyang, S. Zhenmin, W. Jiwu and Z. Caihua, *Chem. Res. Appl.* 13, 157 (2001). (in Chinese)
- [24] N. Faal Hamedani and F. Farzaneh, *J. Sci. Islamic. Rep. of Iran* 17, 231 (2006).
- [25] K. J. Rao, K. Mahesh and S. Kumar, *Bull. Mater. Sci.* 28, 19 (2005). <http://dx.doi.org/10.1007/BF02711166>

- [26] M. Vafae and M.S. Ghamsari, *Mater. Lett.* 61, 3265 (2007). <http://dx.doi.org/10.1016/j.matlet.2006.11.089>
- [27] K. G. Chandrappa, T. V. Venkatesha, K. Vathsala and C. Shivakumara, *J. Nanopart. Res.* 12, 2667 (2010). <http://dx.doi.org/10.1007/s11051-009-9846-0>
- [28] Y. GaoQing, J. Huanfeng, L. Chang and L. ShiJun, *J. Cryst. Growth* 303, 400 (2007).
- [29] E. Boschke, U. Bohmer, J. Lange, M. Constapel, M. Schellentrager and T. Bley, *Chemosphere* 67, 2163 (2007). <http://dx.doi.org/10.1016/j.chemosphere.2006.12.041>
- [30] H. Wang, C. Xie, W. Zhang, S. Cai, Z. Yang and Y. Gui, *J. Hazard. Mater.* 141, 645 (2007). <http://dx.doi.org/10.1016/j.jhazmat.2006.07.021>
- [31] R. Y. Hong, J. H. Li, L. L. Chen, D. Q. Liu, H. Z. Li, Y. Zheng and J. Ding, *Powder Technol.* 189, 426 (2009). <http://dx.doi.org/10.1016/j.powtec.2008.07.004>
- [32] R. M. Trommer, A. K. Alves and C. P. Bergmann, *J. Alloys Compd.* 491, 296 (2010). <http://dx.doi.org/10.1016/j.jallcom.2009.10.147>
- [33] R. Xiangling, H. Dong, C. Dong and T. Fangqiong, *Mater. Res. Bull.* 42, 807 (2007). <http://dx.doi.org/10.1016/j.materresbull.2006.08.030>
- [34] P. Scherrer, *Nachr. Ges. Wiss. Gottingen Math. Phys.* 2, 98 (1918).
- [35] Siqingaowa, Zhaorigetu, Y. Hongxia and Garidi, *Front. Chem. China* 3, 277 (2006). <http://dx.doi.org/10.1007/s11458-006-0036-7>
- [36] L. P. Berube and G. L. Esperance, *J. Electrochem. Soc.* 136, 2314 (1989). <http://dx.doi.org/10.1149/1.2097318>
- [37] M. L. Curri, R. Comparelli, P. D. Cozzoli, G. Mascolo and A. Agostiano, *Mater. Sci. Eng. C* 23, 285 (2003). [http://dx.doi.org/10.1016/S0928-4931\(02\)00250-3](http://dx.doi.org/10.1016/S0928-4931(02)00250-3)